Biomacromolecules

Article

Sensitization of hypoxic tumor to photodynamic therapy via oxygen self-supply of fluorinated photosensitizers

Zhiyong Liu, Yudong Xue, Mengsi Wu, Guoliang Yang, Minbo Lan, and Weian Zhang

Biomacromolecules, **Just Accepted Manuscript** • DOI: 10.1021/acs.biomac.9b01368 • Publication Date (Web): 11 Nov 2019

Sensitization of hypoxic tumor to photodynamic therapy *via* oxygen self-supply of fluorinated photosensitizers

*Zhiyong Liu, Yudong Xue, Mengsi Wu, Guoliang Yang, Minbo Lan, Weian Zhang**

Shanghai Key Laboratory of Functional Materials Chemistry, East China University of Science and Technology.130 Meilong Road, Shanghai 200237, China

KEYWORDS: photodynamic therapy; fluorinated photosensitizers; hypoxic; cancer

ABSTRACT: Photodynamic therapy (PDT) utilizes photosensitizers to convert innoxious oxygen to cytotoxic reactive oxygen species under an appropriate light thus induce cancer cells necrosis. However, PDT performs in an oxygen-dependent method to destroy cells while hypoxia is a feature for most solid tumors. To effectively improve the PDT effect against solid tumors, an oxygen self-supplying and pH-sensitive therapeutic nanoparticle (**PTFC**) has been developed by the self-assembly of a tetrakis(pentafluorophenyl) chlorin (TFPC)-conjugated block copolymer (POEGMA-*b*-P(DEAEMA-*co*-GMA)). **PTFC** nanoparticles can transport oxygen to tumor site with their accumulation in tumor on account of the good oxygen solubility, therefore relieving the oxygen deficiency of solid tumor and enhancing the PDT efficacy. It's worth noting that the oxygen loading was realized by fluorinated photosensitizer itself. In addition, the phototoxicity of **PTFC** nanoparticles is greatly improved in an acidic aqueous environment due to the DEAEMA unit

protonation, which not only enhanced the cellular uptake of nanoparticles but also weakened the aggregation of photosensitizers. Taking the hypoxia and acidic microenvironment of solid tumors, **PTFC** nanoparticles could be efficiently taken up and disassembled to release oxygen upon accumulated at tumor sites, thus significantly improving the PDT efficacy against solid tumors.

INTRODUCTION

Tumor hypoxia, which resulted from overwhelming oxygen consumption, contributes to the growth and metastasis of tumors and impacts their responses to oxygen-consuming therapies, such as photodynamic therapy (PDT), radiotherapy, sonodynamic therapy and chemotherapy (CT).[1-2] Among them, PDT is one of most attractive therapeutic approaches, where oxygen is converted to cytotoxic reactive oxygen species by photoexcited photosensitizers for eliminating tumor cells under a light with a specific wavelength.[3-4] For enhancing the therapeutic effect, a great number of contributions have been recently dedicated to defeating the hypoxia of tumor,[5] including *in situ* oxygen production at tumor sites *via* catalytic reactions,[6-12] oxygen delivery into tumors,[13-19] oxygen-independent photosensitizers for PDT[20-25] as well as hypoxia-reactivated prodrugs for combination therapy of PDT and CT.[26-29] More recently, perfluorocarbons (PFC)-based oxygen delivery systems have attracted much attention for their inherent ability to solubilize oxygen.[30] PFCs are highly hydrophobic and lowly reactive due to the relatively nonpolarity and inertness of the carbon-fluorine bond, endowing them with good biocompatibility and oxygen-dissolving capability.[31] For example, Hu and her *co*-workers developed an oxygen self-enriching PDT system to enhancing the PDT effect against hypoxia tumor by loading photosensitizers into PFC nanodroplets.[32] Shuai and his *co*-workers fabricated an ultrasound /fluorescent bimodal imaging-guided and oxygen-potentiated PDT system by construction of perfluorohexane-cored nanodroplets.[16] Besides, we also reported an oxygen self-sufficient nanosystem through

conjugating PFCs to cyanine 7 for improving combination therapy efficacy of PDT and CT in prior study.[33] Although the antitumor efficiency has been significantly enhanced, the use of PFCs may complicate the preparation process. Hence, it could be an attractive approach to supply oxygen by fluorinated photosensitizer itself.

Another limitation of PDT is that the therapeutic effect is greatly dependent on the effective concentration of photosensitizers. As one of the three elements of photodynamics, most photosensitizers tend to aggregate in aqueous solution due to their poor water solubility, resulting in low tumor selectivity and severely quenched photosensitivity.[34] To overcome this limitation, photosensitizer-based nano-organic frameworks (metal organic frameworks, MOF[35-36] and covalent organic frameworks, COF[37-38]), stimuli-responsive polymeric nanoparticles[39-47] and organic/inorganic hybrid nanoparticles[48-50] have been developed to improve the therapeutic effect of photosensitizers. In consideration of the specific tumor microenvironment (TME), such as low pH,[51-54] over-expressed glutathione,[55-58] enzyme[59-61] or reactive oxygen species,[62-65] significant efforts have been focused on construction of TME-associated stimuli-responsive systems for biologically activatable PDT. Among them, the pH-responsive nanoparticles are of particular interest as a result of the spatiotemporal diversity of pH values in different tissues (e.g. the extracellular environment of tumor (pH 6.5-6.8) is more acidic than that of normal tissues (pH 7.4), and the pH values of intracellular endocytic vesicles are even lower than 6.0.).[66-68] The cell internalization could be effectively improved by activating surface positive charge of nanoparticles at tumor acidic extracellular microenvironment.[69-72] Moreover, photosensitizers can also be selectively activated for enlarged imaging or treatment of tumors through incorporating them into pH-responsive nanoparticles.[73-75] Therefore, it would be of great significance to exploit smart

photosensitizer delivery systems that combine oxygen transport and acid responsiveness for hypoxic tumors.

Herein, we developed an oxygen self-supplying system by the construction of a fluorinated photosensitizer-based POEGMA-*b*-P(DEAEMA-*co*-TFPCMA) (**PTFC**) block copolymer for overcoming the hypoxia of solid tumors, thereby enhancing the photodynamic effect (**Scheme 1**). After amphiphilic **PTFC** block copolymers self-assembled into nanoparticles through hydrophilic and hydrophobic interactions, the hydrophilic shell formed by POEGMA segments endowed **PTFC** nanoparticles with good biocompatibility, which could partially reduce nonspecific cell uptake or protein adsorption during the accumulation of nanoparticles to tumor sites. Due to the high affinity of fluorine to oxygen, oxygen can be effectively adsorbed into the TFPC-containing hydrophobic core and simultaneously delivered to tumor sites with the accumulation of **PTFC** nanoparticles for relieving the hypoxic environment of solid tumors. Moreover, nanoparticles can be more effectively taken up by cancer cells since DEAEMA are pH-responsive resulting in the negative to positive surface charge transition under weak acidic tumor microenvironment. After successful uptake by cells, the nanoparticles can be broken by the lower pH state inside the cells, reducing the aggregation caused quenching (ACQ) effect of photosensitizers. Consequently, the photodynamic effect could be significantly improved by the integration of oxygen transport capacity and pH-responsiveness, where oxygen can be carried by aggregated photosensitizers and then liberated at hypoxia tumor sites, but also, the cellular uptake and photo-sensitiveness of photosensitizers can be improved *via* pH-induced transitions in surface charge and aggregation state of nanoparticles.

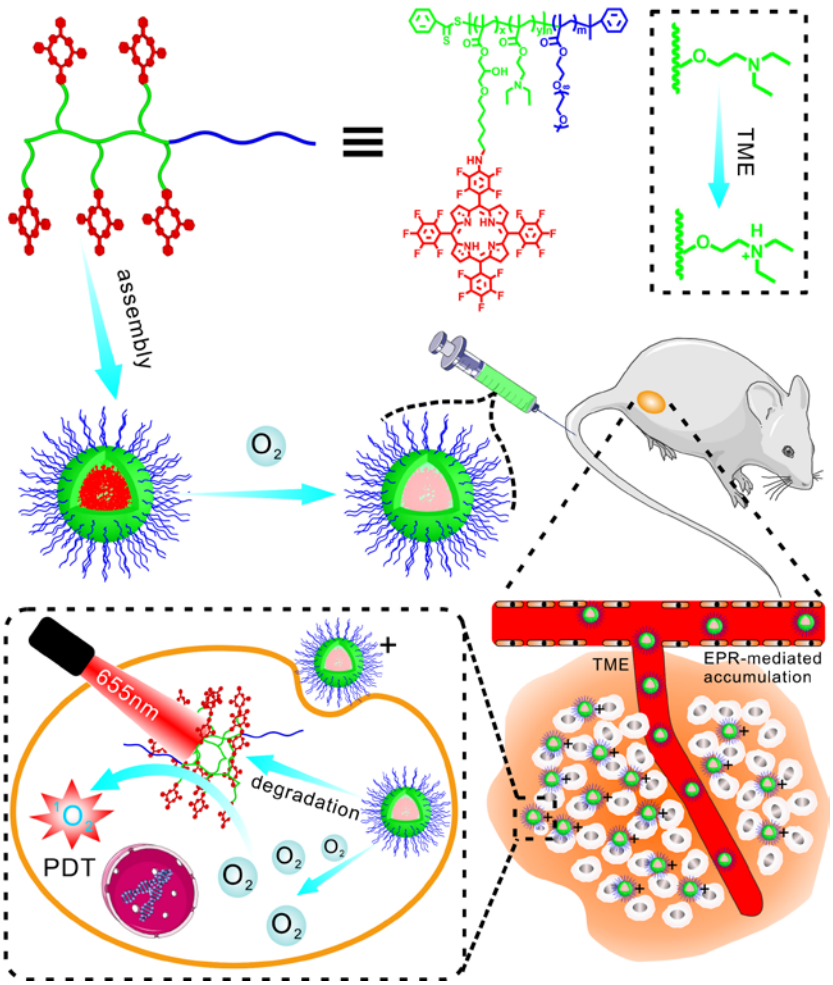

Scheme 1. Schematic illustration of the PTFC nanoparticles formation and the enhancing PDT efficiency resulted from the acidic pH-responsiveness and oxygen transport of PTFC nanoparticles.

EXPERIMENTAL SECTION

Materials. Pentafluoro benzaldehyde and pyrrole were purchased from Macklin Reagents (Shanghai). *p*-Toluenesulfonyl hydrazide was acquired from J&K Scientific Ltd (Shanghai, China). Potassium carbonate (K_2CO_3), sodium sulfate (Na_2SO_4), 1-(3-Dimethylaminopropyl)-3-ethylcarbodiimide hydrochloride (EDC) and 4-dimethylaminopyridine (DMAP) were obtained from Aladdin Reagents of China. Dichloromethane (DCM) and *N*, *N*-dimethylformamide (DMF)

were dried over with calcium hydride (CaH_2) and distilled before use. All other chemicals were directly utilized after they are received without further purification.

Synthesis of TFPP. Pyrrole (268 mg, 4 mmol) and pentafluoro benzaldehyde (784.3 mg, 4 mmol) were dissolved with 300 mL dry dichloromethane in dry and clean flask and then degassed with nitrogen for 30 min. Subsequently, activated molecular sieve (10 mL) and boron trifluoride etherate (47% solution in diethyl ether, 0.3 mL, 1.12 mmol) were added into the DCM solution. The obtained mixture was shielded from ambient light. After stirring for 4 h at room temperature, *p*-tetrachlorobenzoquinone (1 g, 4.06 mmol) was added into the reaction flask and then the mixture was heated to 50 ^{o}C and refluxed for 1 h. Subsequently, the solution containing products were obtained by filtration under reduced pressure and concentrated by vacuum rotary evaporation. The pure product 5, 10, 15, 20-tetrakis-(2, 3, 4, 5, 6-pentafluorophenyl)-porphyrin (TFPP) was obtained by column chromatography (dichloromethane: petroleum ether = 1:4) (400 mg, yield 41%).

Synthesis of TFPP-C6-OH. 100 mg (0.1 mmol) of TFPP was dissolved in mixed solution of tetrahydrofuran (2 mL) and dimethyl sulfoxide (2 mL), 11.8 mg (0.1 mmol) of 6-amino-1-hexanol and 138 mg of K_2CO_3 were added into the above solution. The reaction was performed at room temperature for 4 h and then diluted by dichloromethane and washed with deionized water. The obtained organic layer was dried by anhydrous Na_2SO_4 and then evaporated to obtain dry powder. The powder was further purified by column chromatography elution with dichloromethane to obtain TFPP-C6-OH (30 mg, yield 26 %).

Synthesis of TFPC-C6-OH. 200 mg of TFPP-C6-OH and 1 g of *p*-toluenesulfonyl hydrazide was carefully mixed and then kept under vacuum for 1 h. Subsequently, the reaction was proceeded at 158 ^{o}C for 15 min. After cooling to room temperature, the mixture was dissolved in dichloromethane and then tetrachloro-o-benzoquinone was added into the solution. After the

absorption of at 750 nm disappeared, the solution was washed with a saturated solution of sodium thiosulfate (2×), with distilled water (2×), and then dried over anhydrous Na_2SO_4.

Synthesis of POEGMA Homopolymer and POEGMA-*b*-P(DEAEMA-*co*-GMA) Block Copolymer. OEGMA (1 mL, 2 mmol), CDB (10.8 mg, 0.04 mmol), AIBN (1.3 mg, 0.008 mmol) and 1 mL anhydrous THF were charged in a reaction vial equipped with a magnetic stir bar. The mixture was degassed by several freeze-thaw cycles and sealed in vacuum. Then the reaction was carried out in a preheated oil bath at 70 ^{o}C. After 135 min, the flask was plunged into liquid nitrogen. The reaction solution was dialyzed against pure water and lyophilized under vacuum. $M_{n,\ NMR}$ = 11, 880 g/mol, $M_{n,\ GPC}$ = 6970 g/mol, PDI = 1.05. POEGMA-*b*-P(DEAEMA-*co*-GMA) block Copolymer were synthesized in a similar way by charging POEGMA (100 mg, 10 μmol), DEAEMA (0.15 mL, 0.7 mmol), GMA (0.038mL, 0.3mmol), AIBN (0.1 mL, 3 μmol) and 1 mL anhydrous THF into a reaction vial. After 3.75 h, the flask was plunged into liquid nitrogen. The solution was transferred into a dialysis bag (MWCO, 8000-14000) and dialyzed for 72 h against a mixture of water and THF. Finally, the product-containing solution was frozen and lyophilized under vacuum to afford the white powder. $M_{n,\ NMR}$ = 24, 250 g/mol, $M_{n,\ GPC}$ = 24, 400 g/mol, PDI = 1.15.

Synthesis of PTPP, PTFP and PTFC Block Copolymers. 20 mg of POEGMA-*b*-P(DEAEMA-*co*-GMA) and 35 mg of TFPC-C6-OH were dissolved in 2 mL anhydrous DMF, and then 0.5 mL anhydrous TEA was added into the mixture. The reaction was carried out at room temperature for 14 days under nitrogen atmosphere. Finally, the product **PTFC** copolymer was purified by dialyzing against water and subsequently centrifuging to remove the sediment. **PTFC** copolymer was obtained after lyophilized under vacuum. **PTPP** and **PTFP** copolymers were

synthesized in a similar way by replacing TFPC-C6-OH with TPP-C6-OH and TFPP-C6-OH, respectively.

Self-Assembly PTFP, PTFC and PTPP Copolymers. 5 mg of **PTFC**, **PTFP** and **PTPP** copolymers were separately dissolved in 5 mL of dimethyl formamide. Under vigorous stirring, 1 mL of the solution was added dropwise to deionized water (9 mL) at room temperature. After stirring for 1 h, the organic solvent was removed by dialysis against deionized water for 24 h using a dialysis membrane (MWCO = 3500).

Singlet Oxygen production. As a singlet oxygen scavenger, 1, 3-diphenylisobenzofuran (DPBF) was employed to verify the singlet oxygen production of nanoparticles. A solution containing a fixed concentration nanoparticle and DPBF was added into a quartz cuvette and irradiated at 655 nm for 100 s. The $^1O_2$ generation of nanoparticles can be directly correlated with the decrease of the DPBF absorbance in the UV-vis spectrum, thus the absorbance of DPBF at 415 nm was measured every 20 s.

Cell Culture. 4T1 murine breast cancer cells were cultivated in Dulbecco's modified Eagle's medium (DMEM) supplemented with 1% antibiotics (penicillin and streptomycin) and 10% fetal bovine serum (FBS) in a humidified standard atmosphere of 5% CO_2 at 37 ^oC.

Intracellular ROS Generation Assay. Dichlorofluorescein diacetate (DCFH-DA) was employed as a probe to measure the intracellular ROS production. The ROS-induced oxidation of DCFH-DA could result in the generation of highly fluorescent DCF. Typically, 4T1 cells with a density of 1×10^5 containing complete DMEM media were incubated on glass bottom cell culture dish for 24 h. Then, the 4T1 cells were chosen to incubate with **PTFP**, **PTFC** or **PTPP** nanoparticles for 24 h with or without light irradiation (655 nm, 10 min, 100 mW/cm^2). The group without any treatment was acted as the control. The cells medium was replaced with DMEM

containing DCFH-DA solution at the concentration of 10×10^{-6} M at 37 ºC in dark. After treatment for 30 min the cells were observed *via* confocal laser scanning microscopy (CLSM) to evaluate the ROS generation. The excitation wavelength was 488 nm and the emission wavelength was 525 nm for the DCFH-DA detection.

Cellular Uptake Evaluation. The cellular uptake was determined by the utilization of CLSM. 4T1cells (2×10^4 cells/well) were seed on glass bottom cell culture dish for 24 h, and then the cells were cultured with fresh medium containing **PTFP**, **PTFC** or **PTPP** nanoparticles at the same concentration 50 μmol/mL of porphyrin for 24 h. Next, the cells were washed carefully with PBS and then treated with 4% paraformaldehyde. After paraformaldehyde was removed, hoechst were utilized to stain the cells nuclei for 3 min and the staining were terminated by washing three times with PBS. Finally, intracellular fluorescence of porphyrin was observed by CLSM with excitation at 404 nm and emission at 660 nm.

Cytotoxicity Assay. The cytotoxicity of **PTFC** nanoparticles was evaluated by a standard MTT assay. 200 μL of 4T1 cell suspension (1×10^4 cells/mL) was seeded in a 96-well plate and then incubated for 24 h at 37 ºC. Different concentrations of **PTFP**, **PTFC** and **PTPP** nanoparticles in fresh DMEM media were added into the wells and co-cultured for another 24 h. The cells were washed and irradiated with 660 nm laser (200 mW/cm^2) for 10 min. Before the media was replaced with 200 μL of MTT solution (0.5 mg/mL in DMEM) and cultured for 4 h, the cells were incubated for further 24 h. Finally, 150 μL of DMSO per well was added to replace the MTT solution and dissolve the formazan, and the absorbance value was recorded with a SpectraMax spectrometer at the wavelength of 492 nm. The *in vitro* dark cytotoxicity of nanoparticles was checked using the same procedure described above but without illumination.

Animals and Tumor Xenograft Model. BALB/c mice bearing xenograft tumor were established and employed for *in vivo* imaging and PDT performance: 200 μL of 4T1 cells in PBS (5×10^7 cells/mL) were subcutaneously injected into the mice, respectively. The tumor volumes (V) were measured by the length and width of tumors and calculated as V = 0.5 × (tumor length) × (tumor width)^2. Relative tumor volume was defined as V/V_0 (V_0 was the tumor volume when the treatment was initiated). All animal studies were conducted on male Balb/c nude mice (four to five weeks) in compliance with the National Institutes of Health Guide for the Care and Use of Laboratory Animals approved by the Animal Ethics Committee of the East China University of Science & Technology.

***In vivo* Fluorescence Imaging.** For fluorescence imaging, mice with 4T1 tumor were administrated with 200 μL of nanoparticles labeled by Cy7 (1 mg/mL of porphyrin) through the tail vein. All the image acquisitions were performed with *in vivo* multispectral imaging system (Kodak FX) equipped with excitation bandpass filter at 750 nm and emission 830 nm when the mice were anesthetized at 0.5 h, 2 h, 4 h, 6 h, 12 h, 24 h, and 36 h post-injection.

***In vivo* Therapeutical Evaluation of PTFC Nanoparticles.** The 4T1 tumor-bearing mice were chosen for therapeutical evaluation of the PTFC nanoparticles. After the tumor volumes of the 4T1 tumor-bearing mice reached about 100 mm^3, the mice were divided into five group (n=4 for each group) and administrated with different agents: (1) **Control**, (2) **PTPP**, (3) **PTFC**, (4) **PTPP + laser**, (5) **PTFC + laser** (porphyrin concentration at 1 mg/kg). The power density of 655 nm laser was 200 mW/cm^2. The tumor volumes were measured by vernier caliper every two days. The body weights of mice were recorded during the whole experiments. The mice were sacrificed at day 18 and the tumors were dissected and weighed. The dissected tumors of the groups (1) **Control**, (2) **PTPP**, (3) **PTFC**, (4) **PTPP + laser**, (5) **PTFC + laser** were embedded in paraffin and made as

slices by cryotomy. Furthermore, the frozen slices were stained with H&E and imaged under an inverted fluorescence microscope to further characterize the therapeutic effects.

RESULTS AND DISCUSSION

Synthesis and Self-assembly of PTFC. To fabricate the pH-responsive oxygen-carrying **PTFC** nanoparticles, the fluorinated photosensitizer, 5-((2,3,5,6-tetrafluoro-4-((6-hydroxyhexyl) amino) phenyl)-10, 15, 20-tri(perfluorophenyl) chlorin (abbreviated as TFPC-C6-OH) and pH-responsive block copolymer (POEGMA-*b*-P(DEAEMA-*co*-GMA)) were prepared, respectively. First, we synthesized TFPC-C6-OH by the diamine reduction of 5-((2, 3, 5, 6-tetrafluoro-4-((6-hydroxyhexyl) amino) phenyl)-10, 15, 20-tri(perfluorophenyl) porphyrin (TFPP-C6-OH), which was obtained by the nucleophilic substitution of tetrafluorophenyl porphyrin (TFPP) with 6-amino-1-hexanol (**Scheme S1**).[76] The successful syntheses of above compounds were verified by proton and fluorine nuclear magnetic resonance spectrometry measurements as shown in **Figure S1-S5**. Next, pH-responsive block copolymer (POEGMA-*b*-P(DEAEMA-*co*-GMA)) was prepared through RAFT polymerization (**Scheme S2**). Oligo ethylene glycol methacrylate (OEGMA) monomers were polymerized with cumyldithiobenzoate to form the hydrophilic POEGMA homopolymer, and then POEGMA as a macro-RAFT agent was used for copolymerization of glycidyl methacrylate and 2-(diethylamino)ethyl methacrylate to produce the POEGMA-*b*-P(DEAEMA-*co*-GMA) block copolymer. Gel permeation chromatography (GPC) and ^{1}H NMR were employed to characterize the structures and molecular weights of these polymers, respectively (**Figure S6-S8**). We found that the GPC traces of POEGMA and POEGMA-*b*-P(DEAEMA-*co*-GMA) were symmetrical, suggesting the polymerizations proceeded in a living manner. The average molecular weight calculated from ^{1}H NMR was in line with that from GPC. Finally, **PTFC** was obtained by conjugating TFPC-C6-OH to POEGMA-*b*-

P(DEAEMA-*co*-GMA) through ring-opening reaction of hydroxyl and epoxy group. Meanwhile, POEGMA-*b*-P(DEAEMA-*co*-**PTFP**MA) (**PTFP**) and POEGMA-*b*-P(DEAEMA-*co*-TPPMA) (**PTPP**) block copolymers were also prepared in a similar way by replacing TFPC-C6-OH with TFPP-C6-OH or TPP-C6-OH, respectively. Detailed synthesis process and characterization were given in supporting information (**Scheme S3-S5** and **Figure S9-S11**).

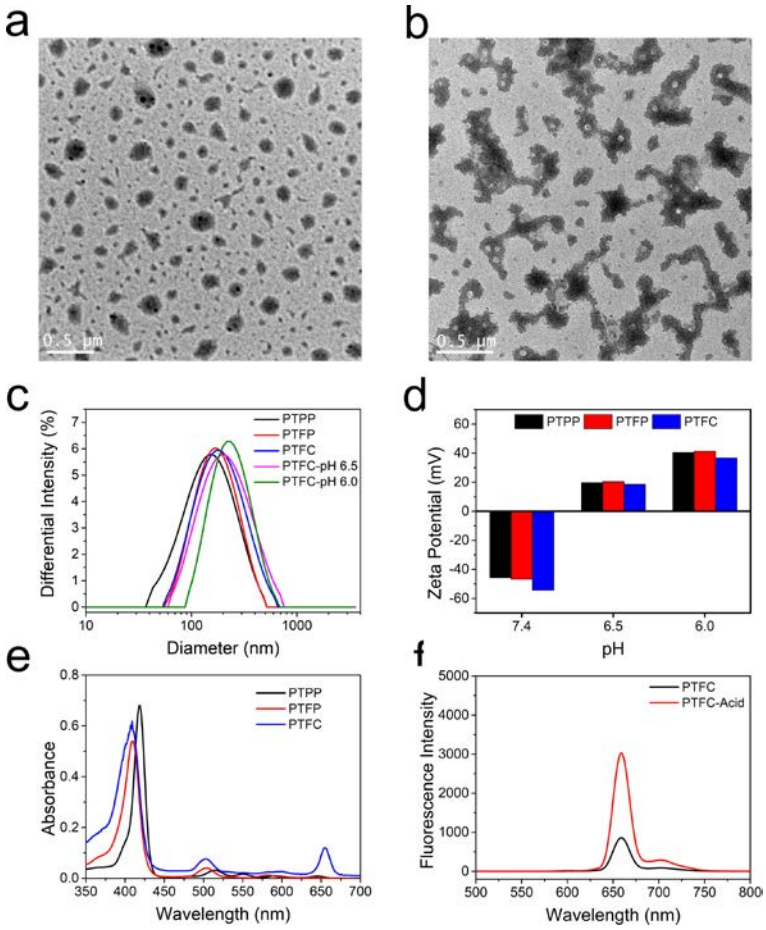

Figure 1. TEM images of **PTFC** nanoparticles in different condition (a) pH = 7.4, (b) pH = 6.0. (c) Size distribution of nanoparticles determined by DLS. (d) Zeta potential of nanoparticles under different conditions. (e) Absorbance spectra and (f) emission spectra of **PTFC** nanoparticles.

The nanoparticles were prepared by a nanoprecipitation method. Briefly, the POEGMA-*b*-P(DEAEMA-*co*-TFPCMA), POEGMA-*b*-P(DEAEMA-*co*-TFPPMA) and POEGMA-*b*-

P(DEAEMA-*co*-TPPMA) block copolymers were separately dissolved in tetrahydrofuran (THF), and then these THF solutions were added drop by drop into deionized water under rapid stirring. Finally, after removal of THF through dialysis against ultrapure water, the corresponding nanoparticles were obtained and abbreviated as **PTFC**, **PTFP** and **PTPP**, respectively. Transmission electron microscopy (TEM) was utilized to observe the morphology of nanoparticles, as depicted in **Figure 1a**, **S12** and **S13**. We found **PTFC**, **PTFP** and **PTPP** nanoparticles dispersed in PBS at pH 7.4 were all sphere-like and had an average diameter of 160 nm, 165 nm and 170 nm, respectively. However, when the nanoparticles were stored in PBS at pH 6.0 (acidic microenvironment), the assembled aggregates became irregular as shown in **Figure 1b**, which might be resulted from the hydrophobic to hydrophilic transformation of copolymers through the protonation of DEAEMA units. The diameter distribution of nanoparticles was also characterized by dynamic light scattering (DLS) as displayed in **Figure 1c**. In PBS at pH 7.4, the hydrodynamic diameters of **PTFC**, **PTFP** and **PTPP** nanoparticles were 171 nm (PDI = 0.21), 173 nm (PDI = 0.23) and 174 nm (PDI = 0.24). In addition, the size of nanoparticles increased gradually with the pH decrease, due to the responsive ability of nanoparticles to acid microenvironment. These consequences matched well with those of TEM. Zeta potential was further utilized to determine responsiveness of the nanoparticles to acid pH as shown in **Figure 1d**. The potentials of all nanoparticles were negative and lower than -40 mV at pH = 7.4, while they were positive under acidic condition and even higher than 30 mV at pH = 6.0. This outcome suggested that the cell uptake of pH-responsive nanoparticles may be facilitated at acid tumor site due to the charge reverse. Absorption (**Figure 1e**) and fluorescence emission spectra (**Figure 1f**) of nanoparticles were measured as well. It can be seen that **PTFC** nanoparticles have a strong absorption peak in red light region thus **PTFC** is beneficial for PDT of deep-seated tumor.

Meanwhile, the fluorescence intensity of **PTFC** under acid condition is significantly higher than that under neutral condition, indicating that the aggregation-induced quenching effect of photosensitizers in **PTFC** nanoparticles could be greatly weakened. As a consequence, **PTFC** nanoparticles should be efficient for performing PDT against solid tumors.

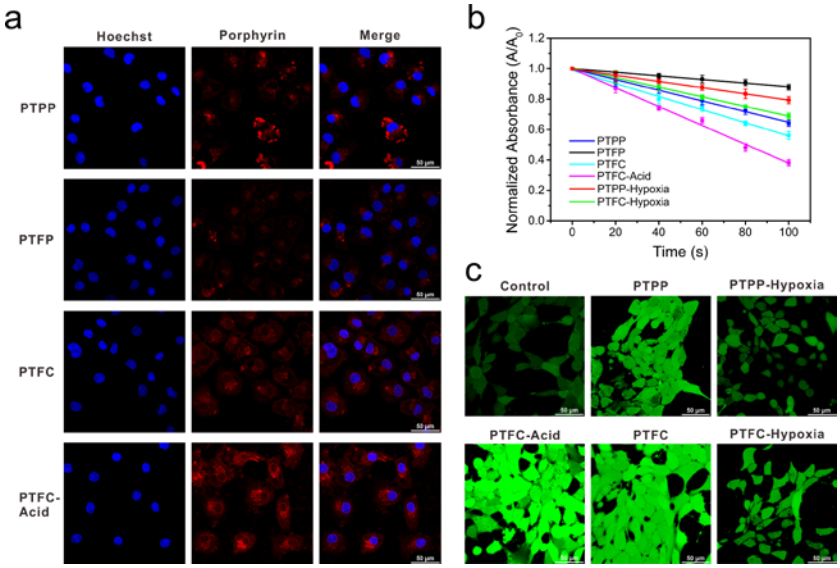

Figure 2. Cell internalization and ROS generation. (a) CLSM images of 4T1 cells incubated with **PTPP**, **PTFP** and **PTFC** nanoparticles under physiological conditions (pH = 7.4) or acidic condition (pH = 6.5). (b) Extracellular ROS generation detected by DPBF (n = 3, mean ± s.d.) and (c) fluorescence images of ROS generation in 4T1 cells treated with nanoparticles, as detected with DCFH-DA.

Extracellular and Intracellular ROS Production and Cellular Internalization. To achieve effective PDT, photosensitizers need to be effectually taken up by cells. Therefore, the cell uptake ability of obtained nanoparticles was first explored using 4T1 cells as a model. Confocal laser scanning microscope (CLSM) was employed to evaluate the uptake of nanoparticles by cells *via* detecting the fluorescence of porphyrin as shown in **Figure 2a**. The intracellular red fluorescence of porphyrin indicated nanoparticles could be successfully internalized by 4T1 cells. Moreover,

the amount of endocytosed nanoparticles at acid condition was significantly higher than that at normal condition, which was confirmed by the stronger intracellular fluorescence of nanoparticles. These results showed the nanoparticles could be used as a potential carrier of photosensitizers for PDT.

Encouraged by the excellent internalization capacity of the nanoparticles, we next investigated the photoinduced extracellular and intracellular ROS production of the nanoparticles under 655 nm laser. For extracellular ROS production, 1, 3-diphenylisobenzofuran (DPBF) was utilized as a ROS indicator.[77] The characteristic absorption of DPBF at around 415 nm was detected by an ultraviolet detector to indicate the generated ROS by the nanoparticles under light illumination. As shown in **Figure 2b**, both **PTFC** and **PTPP** nanoparticles could result in obvious decrease of absorbance of DPBF at 415 nm, however, **PTFP** nanoparticles showed almost no variation. These results could be attributed to the absorbance differences between **PTFP** with **PTFC** and **PTPP** nanoparticles, indicating that the diamine reduction of TFPP could significantly enhance the PDT ability of TFPP in red light region. In addition, the decrease rate of DPBF of **PTFC** nanoparticles was faster than that of **PTPP** nanoparticles, which may be induced by the oxygen-carrying capacity of **PTFC** nanoparticles. To confirm our hypothesis, we also investigated the ROS generation of **PTFC** and **PTPP** nanoparticles under hypoxia. It can be seen that the ROS production of **PTPP** nanoparticles was strongly inhibited while that of **PTFC** nanoparticles was still remarkable, demonstrating that **PTFC** nanoparticles have the good oxygen-carrying capacity. The oxygen-carrying capacity was further confirmed by testing the dissolved oxygen through using a dissolved oxygen detector. As shown in **Figure S14**, **PTFC** and **PTFP** nanoparticles both showed higher dissolved oxygen value in comparison with the control without fluorine (**PTPP**). Finally, we further explored the ROS production of **PTFC** nanoparticles under acid condition, the most rapid

decay of the absorbance of DPBF was observed, indicating that the aggregation of porphyrin in nanoparticles could be effectively attenuated by the protonation of DEAEMA units.

As for the intracellular ROS production, it was observed *via* CLSM using DCFH-DA as a ROS indicator as shown in **Figure 2c** and **Figure S15**. In contrast to the control, strong green fluorescence intensity was observed in both **PTFC** and **PTPP** nanoparticles upon irradiation with 655 nm laser while that of **PTFP** nanoparticles was no obvious change, which was in line with the extracellular result of ROS production. When the cells were incubated with the nanoparticles under hypoxia, the generation of ROS of **PTFC** were slightly restrained compared to that under normoxia while fluorescence intensity of **PTPP** was almost same as the control, indicating that **PTFC** nanoparticles could carry oxygen thus enhancing the PDT effect under hypoxia. More importantly, for the cells cultured with **PTFC** nanoparticles in acidic medium, we found the green fluorescence intensity was significantly increased after irradiated with 655 nm laser, demonstrating prominent production of ROS. In consideration of all the above results, **PTFC** nanoparticles could be a potential system for PDT against solid tumors.

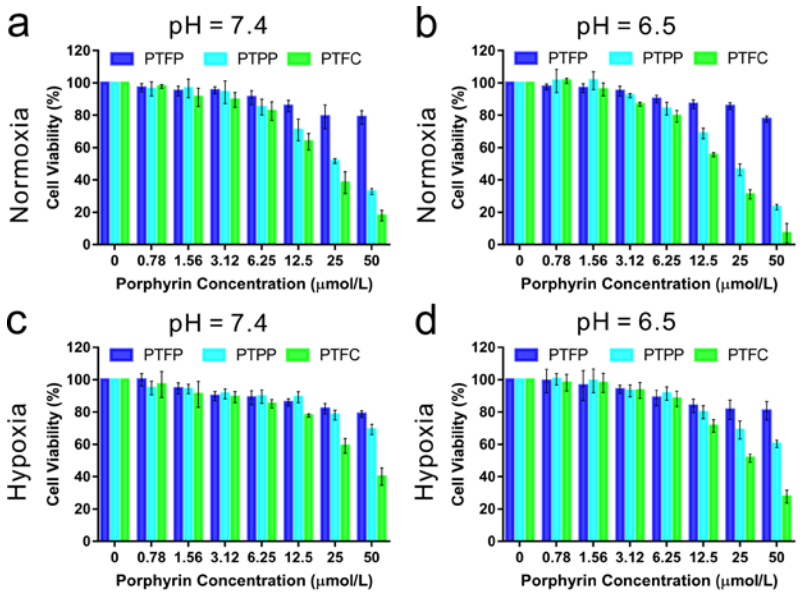

Figure 3. Photo-cytotoxicity studies by MTT assay for 4T1 cells after incubation with various concentrations of different nanoparticles. (a) Normoxia conditions (pH = 7.4), (b) normoxia and acid (pH = 6.5) condition, (c) hypoxia condition (pH = 7.4) and (d) hypoxia and acid (pH = 6.5) condition. (n = 3, mean ± s.d.).

***In vitro* Cytotoxicity Assay.** To investigate the antitumor ability of **PTFC** nanoparticles, the cytotoxicity of nanoparticles was performed *via* MTT assay under different conditions (normoxia, hypoxia or acid condition). We first investigated the cytotoxicity of nanoparticles without laser irradiation as shown in **Figure S16**, and it can be seen that all the nanoparticles did not showcase obvious toxicity after cultured with 4T1 cells for 24 h even under hypoxia and acid condition. These results indicated that the obtained nanoparticles have a good biocompatibility. Next, the photodynamic antitumor effect was verified by laser illumination at 655 nm for 10 min after the 4T1 cells were incubated with the nanoparticles for 24 h. Under normoxia, the cell viabilities decreased with increased concentration of both **PTFC** and **PTPP** nanoparticles at pH = 7.4 (**Figure 3a**), and a similar result was observed at pH = 6.5 (**Figure 3b**) with a more significant inhibiting effect. These consequences demonstrated the nanoparticles have a higher phototoxicity in acid environment. Moreover, the lowest viabilities were observed in cells treated with **PTFC** nanoparticles at both pH = 7.4 and pH = 6.5, which may be resulted from the oxygen self-supply of **PTFC** nanoparticles. Subsequently, the phototoxicities of the nanoparticles were performed under hypoxia at pH = 7.4 or pH = 6.5 as well. As shown in **Figure 3c**, the cell viabilities were higher compared to that under normoxia. **PTPP** nanoparticles showed extremely weak toxicity against tumor cells while the cell viability treated by **PTFC** nanoparticles even reduced to around 40%, indicating the antitumor effect of **PTFC** nanoparticles was evidently stronger than that of **PTPP** nanoparticles. All these results revealed that the **PTFC** nanoparticles could also efficiently

destroy tumor cells under hypoxia. The similar consequences were also found under hypoxia at pH = 6.5 (**Figure 3d**), and the antitumor effect of PDT was slightly enhanced as compared with that at pH = 7.4, suggesting that the phototoxicity of the nanoparticles could be amplified under acidic condition. As a control, **PTFP** nanoparticles showed almost no toxic in all conditions after exposing to 655 nm laser. As a consequence, the amplified PDT effect may be well realized *via* **PTFC** nanoparticles in hypoxia and acidic tumors.

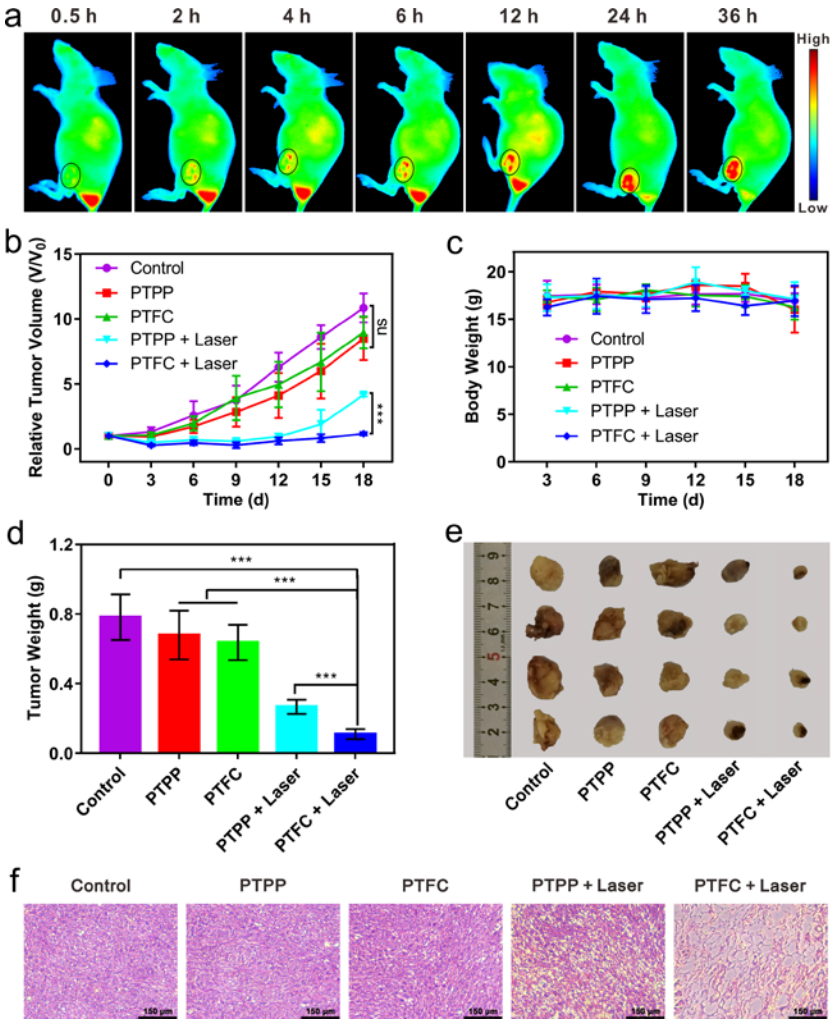

Figure 4. *In vivo* fluorescence imaging and PDT performance of intravenously injected **PTFC** nanoparticles in mice bearing 4T1 subcutaneous tumor model. (a) Fluorescence imaging for different times. (b) Relative tumor volume and (c) body weight change during the treatment. (d)

Average weight of representative tumors. (e) Photographs of the tumor dissection. (f) Pictures of H&E stained tumors. (n = 4, mean ± s.d. ***$p < 0.005$).

***In vivo* Fluorescence Imaging and Anticancer Efficacy of PTFC.** To further demonstrate the excellent PDT effect of **PTFC** nanoparticles, the BALB/c mice bearing xenografted tumor were fabricated by injecting with 4T1 tumor cells subcutaneously for performing *in vivo* PDT. The nanoparticles were injected into 4T1 tumor-bearing mice *via* the tail vein when tumor volume reached to about 100 mm^3 for investigating the accumulation and antitumor effect *in vivo*. The accumulation of nanoparticles was real-time recorded by *in vivo* fluorescence imaging after the cyanine (Cy7)-labelled nanoparticles were given through tail vein injection as shown in **Figure 4a**. The increased fluorescence intensity was observed with the extension of time, which could be ascribed to the enhanced permeability and retention (EPR) effect of tumors. This result indicated that the size of nanoparticles was suitable as a delivery system for achieving successfully cargo transport to tumor sites. The highest fluorescence intensity was observed at 24 h post-injection and could be kept even at 36 h post-injection. Therefore, it would be an optimal method to perform antitumor test after the nanoparticles were given for 1 d.

Tumor-bearing mice were randomly divided into five groups (the control, **PTPP**, **PTFC**, **PTPP + Laser** and **PTFC + Laser**) and then administrated with saline, **PTPP** or **PTFC** nanoparticles, respectively. Mice in **PTPP + Laser** and **PTFC + Laser** groups were illuminated with 655 nm laser for 10 min after 24 h of the administration to determine the antitumor PDT effect, while **PTPP** and **PTFC** groups were used as contrast groups to verify the biocompatibility of the nanoparticles. **Figure 4b** revealed **PTFC** nanoparticles mediated PDT exhibited the most significant inhibition effect to tumors at day 18 after light illumination. In contrast, we found **PTPP** nanoparticles showed a modest therapeutic effect to tumors. The remarkable antitumor effect of

PTFC nanoparticles may benefit from its oxygen-carrying ability. Moreover, **PTPP** and **PTFC** nanoparticles both demonstrated that there was almost no impact on the tumor growth without laser irradiation, which could be ascribed to the well biocompatibility of these nanoparticles. In addition, the body weights of all mice were recorded in **Figure 4c** and there was also no significant change during PDT treatments, indicating the nanoparticles had no obvious systemic toxicity. The tumors were excised from tumor-bearing mice at day 18 after the treatment to further investigate the tumor inhibition effect. As shown in **Figure 4d** and **4e**, the mean tumor weight and size of all groups indicated that the greatest inhibition effect was well carried out by **PTFC** nanoparticles, which was in agreement with the former results. The antitumor efficacy and biocompatibility were also investigated *via* hematoxylin and eosin (H&E) staining of excised tumors and main organs, respectively. The pictures of H&E stained tumors (**Figure 4f**) demonstrated that **PTFC** nanoparticles resulted in prominent necrosis to tumor under laser illumination, which further confirmed the significant PDT effect of **PTFC** nanoparticles. As proved by H&E staining of major organs (**Figure S17**), there was no obvious tissue destruction to the major organs of mice injected with the nanoparticles, which suggested that these nanoparticles were high biocompatible.

CONCLUSIONS

In summary, we fabricated an oxygen self-suppling system by conjugating a far-red-absorbing fluorinated photosensitizers (TFPC) to a pH-responsive block copolymer (POEGMA-*b*-P(DEAEMA-*co*-GMA) for sensitization of hypoxic tumor to PDT. The block copolymers can form **PTFC** nanoparticles with an appropriate size to accumulate at tumor site by EPR effect. The hypoxia tumor environment can be improved through the release of oxygen carried by nanoparticles, the oxygen carry was well realized by photosensitizers itself without the additional

reagent such as perfluorocarbons. Moreover, due to the pH-responsive ability, the uptake of nanoparticles can be effectively improved and the aggregation of photosensitizers can be attenuated as well, leading to enhanced PDT effect. Thus, the efficient PDT can be well realized by **PTFC** nanoparticles, which incorporated the oxygen-carrying ability and acidic responsiveness. This work offers a smart nano-photosensitizer with effective regulation of tumor microenvironment and activation of photosensitizers to realize a safer and more reliable PDT efficacy.

ASSOCIATED CONTENT

Supporting Information.

The Supporting Information is available free of charge on the ACS Publications website at DOI: 10.1021/acs.biomac

Figures S1−S17 of the following data: additional TEM, ^{1}H NMR and ^{19}F NMR spectrum, GPC, and CLSM images, and cell viability (PDF).

AUTHOR INFORMATION

Corresponding Author

*E-mail: wazhang@ecust.edu.cn

Notes

The authors declare no competing financial interest.

ACKNOWLEDGMENT

This work was financially supported by the National Natural Science Foundation of China (No. 21574039 and 21875063).

REFERENCES

(1) Wilson, W. R.; Hay, M. P., Targeting hypoxia in cancer therapy. *Nat. Rev. Cancer* **2011**, *11*, 393-410.

(2) Li, X.; Kwon, N.; Guo, T.; Liu, Z.; Yoon, J., Innovative Strategies for Hypoxic-Tumor Photodynamic Therapy. *Angew. Chem. Int. Ed.* **2018**, *57*, 11522-11531.

(3) Luby, B. M.; Walsh, C. D.; Zheng, G., Advanced Photosensitizer Activation Strategies for Smarter Photodynamic Therapy Beacons. *Angew. Chem. Int. Ed.* **2019**, *58*, 2558-2569.

(4) Yang, M.; Yang, T.; Mao, C., Enhancement of Photodynamic Cancer Therapy by Physical and Chemical Factors. *Angew. Chem. Int. Ed.* **2019**, *58*, 14066-14080.

(5) Dang, J.; He, H.; Chen, D.; Yin, L., Manipulating tumor hypoxia toward enhanced photodynamic therapy (PDT). *Biomater. Sci.* **2017**, *5*, 1500-1511.

(6) Meng, L.; Cheng, Y.; Tong, X.; Gan, S.; Ding, Y.; Zhang, Y.; Wang, C.; Xu, L.; Zhu, Y.; Wu, J.; Hu, Y.; Yuan, A., Tumor Oxygenation and Hypoxia Inducible Factor-1 Functional Inhibition via a Reactive Oxygen Species Responsive Nanoplatform for Enhancing Radiation Therapy and Abscopal Effects. *ACS Nano* **2018**, *12*, 8308-8322.

(7) Yao, C.; Wang, W.; Wang, P.; Zhao, M.; Li, X.; Zhang, F., Near-Infrared Upconversion Mesoporous Cerium Oxide Hollow Biophotocatalyst for Concurrent pH-/H2 O2 -Responsive O2 -Evolving Synergetic Cancer Therapy. *Adv. Mater.* **2018**, *30*, 1704833.

(8) Zhang, Y.; Wang, F.; Liu, C.; Wang, Z.; Kang, L.; Huang, Y.; Dong, K.; Ren, J.; Qu, X., Nanozyme Decorated Metal-Organic Frameworks for Enhanced Photodynamic Therapy. *ACS Nano* **2018**, *12*, 651-661.

(9) Zhang, X.; Xi, Z.; Machuki, J. O.; Luo, J.; Yang, D.; Li, J.; Cai, W.; Yang, Y.; Zhang, L.; Tian, J.; Guo, K.; Yu, Y.; Gao, F., Gold Cube-in-Cube Based Oxygen Nanogenerator: A Theranostic Nanoplatform for Modulating Tumor Microenvironment for Precise Chemo-Phototherapy and Multimodal Imaging. *ACS Nano* **2019**, *13*, 5306-5325.

(10) Phua, S. Z. F.; Yang, G.; Lim, W. Q.; Verma, A.; Chen, H.; Thanabalu, T.; Zhao, Y., Catalase-Integrated Hyaluronic Acid as Nanocarriers for Enhanced Photodynamic Therapy in Solid Tumor. *ACS Nano* **2019**, *13*, 4742-4751.

(11) Chen, Q.; Feng, L.; Liu, J.; Zhu, W.; Dong, Z.; Wu, Y.; Liu, Z., Intelligent Albumin-MnO2 Nanoparticles as pH-/H2 O2 -Responsive Dissociable Nanocarriers to Modulate Tumor Hypoxia for Effective Combination Therapy. *Adv. Mater.* **2016**, *28*, 7129-7136.

(12) Li, J.; Wei, K.; Zuo, S.; Xu, Y.; Zha, Z.; Ke, W.; Chen, H.; Ge, Z., Light-Triggered Clustered Vesicles with Self-Supplied Oxygen and Tissue Penetrability for Photodynamic Therapy against Hypoxic Tumor. *Adv. Funct. Mater.* **2017**, *27* , 1702108.

(13) Que, Y. R.; Liu, Y. J.; Tan, W.; Feng, C.; Shi, P.; Li, Y. J.; XiaoyuHuang, Enhancing Photodynamic Therapy Efficacy by Using Fluorinated Nanoplatform. *Acs Macro Lett.* **2016**, *5*, 168-173.

(14) Hu, D. R.; Zhong, L.; Wang, M. Y.; Li, H. H.; Qu, Y.; Liu, Q. Y.; Han, R. X.; Yuan, L. P.; Shi, K.; Peng, J. R.; Qian, Z. Y., Perfluorocarbon-Loaded and Redox-Activatable Photosensitizing

Agent with Oxygen Supply for Enhancement of Fluorescence/Photoacoustic Imaging Guided Tumor Photodynamic Therapy. *Adv. Funct. Mater*. **2019**, *29*, 1806199.

(15) Song, G.; Liang, C.; Yi, X.; Zhao, Q.; Cheng, L.; Yang, K.; Liu, Z., Perfluorocarbon-Loaded Hollow Bi2Se3 Nanoparticles for Timely Supply of Oxygen under Near-Infrared Light to Enhance the Radiotherapy of Cancer. *Adv. Mater*. **2016**, *28*, 2716-2723.

(16) Yu, M.; Xu, X.; Cai, Y.; Zou, L.; Shuai, X., Perfluorohexane-cored nanodroplets for stimulations-responsive ultrasonography and O2-potentiated photodynamic therapy. *Biomaterials* **2018**, *175*, 61-71.

(17) Hu, H.; Yan, X.; Wang, H.; Tanaka, J.; Wang, M.; You, W.; Li, Z., Perfluorocarbon-based O2 nanocarrier for efficient photodynamic therapy. *J. Mater. Chem. B* **2019**, *7*, 1116-1123.

(18) Song, X.; Feng, L.; Liang, C.; Yang, K.; Liu, Z., Ultrasound Triggered Tumor Oxygenation with Oxygen-Shuttle Nanoperfluorocarbon to Overcome Hypoxia-Associated Resistance in Cancer Therapies. *Nano Lett.* **2016**, *16*, 6145-6153.

(19) Xu, S.; Zhu, X.; Zhang, C.; Huang, W.; Zhou, Y.; Yan, D., Oxygen and Pt(II) self-generating conjugate for synergistic photo-chemo therapy of hypoxic tumor. *Nat. Commun.* **2018**, *9*, 2053.

(20) Li, M.; Xia, J.; Tian, R.; Wang, J.; Fan, J.; Du, J.; Long, S.; Song, X.; Foley, J. W.; Peng, X., Near-Infrared Light-Initiated Molecular Superoxide Radical Generator: Rejuvenating Photodynamic Therapy against Hypoxic Tumors. *J. Am. Chem. Soc.* **2018**, *140*, 14851-14859.

(21) Li, M. D.; Wong, N. K.; Xiao, J.; Zhu, R.; Wu, L.; Dai, S. Y.; Chen, F.; Huang, G.; Xu, L.; Bai, X.; Geraskina, M. R.; Winter, A. H.; Chen, X.; Liu, Y.; Fang, W.; Yang, D.; Phillips, D. L.,

Dynamics of Oxygen-Independent Photocleavage of Blebbistatin as a One-Photon Blue or Two-Photon Near-Infrared Light-Gated Hydroxyl Radical Photocage. *J. Am. Chem. Soc.* **2018**, *140*, 15957-15968.

(22) Zhang, C.; Yan, L.; Wang, X.; Dong, X.; Zhou, R.; Gu, Z.; Zhao, Y., Tumor Microenvironment-Responsive Cu2(OH)PO4 Nanocrystals for Selective and Controllable Radiosentization via the X-ray-Triggered Fenton-like Reaction. *Nano Lett.* **2019**, *19*, 1749-1757.

(23) Li, X.; Lee, D.; Huang, J. D.; Yoon, J., Phthalocyanine-Assembled Nanodots as Photosensitizers for Highly Efficient Type I Photoreactions in Photodynamic Therapy. *Angew. Chem. Int. Ed.* **2018**, *57*, 9885-9890.

(24) Gilson, R. C.; Black, K. C. L.; Lane, D. D.; Achilefu, S., Hybrid TiO2 -Ruthenium Nano-photosensitizer Synergistically Produces Reactive Oxygen Species in both Hypoxic and Normoxic Conditions. *Angew. Chem. Int. Ed.* **2017**, *56*, 10717-10720.

(25) Zhang, K.; Yu, Z.; Meng, X.; Zhao, W.; Shi, Z.; Yang, Z.; Dong, H.; Zhang, X., A Bacteriochlorin-Based Metal-Organic Framework Nanosheet Superoxide Radical Generator for Photoacoustic Imaging-Guided Highly Efficient Photodynamic Therapy. *Adv. Sci.* **2019**, *6*, 1900530.

(26) Yang, S.; Tang, Z.; Hu, C.; Zhang, D.; Shen, N.; Yu, H.; Chen, X., Selectively Potentiating Hypoxia Levels by Combretastatin A4 Nanomedicine: Toward Highly Enhanced Hypoxia-Activated Prodrug Tirapazamine Therapy for Metastatic Tumors. *Adv. Mater.* **2019**, *31*, 1805955.

(27) Park, W.; Bae, B. C.; Na, K., A highly tumor-specific light-triggerable drug carrier responds to hypoxic tumor conditions for effective tumor treatment. *Biomaterials* **2016**, *77*, 227-234.

(28) Wang, W.; Cheng, Y.; Yu, P.; Wang, H.; Zhang, Y.; Xu, H.; Ye, Q.; Yuan, A.; Hu, Y.; Wu, J., Perfluorocarbon regulates the intratumoural environment to enhance hypoxia-based agent efficacy. *Nat. Commun.* **2019**, *10*, 1580.

(29) Zhu, R.; He, H.; Liu, Y.; Cao, D.; Yan, J.; Duan, S.; Chen, Y.; Yin, L., Cancer-Selective Bioreductive Chemotherapy Mediated by Dual Hypoxia-Responsive Nanomedicine upon Photodynamic Therapy-Induced Hypoxia Aggravation. *Biomacromolecules* **2019**, *20*, 2649-2656.

(30) Zhuang, J.; Ying, M.; Spiekermann, K.; Holay, M.; Zhang, Y.; Chen, F.; Gong, H.; Lee, J. H.; Gao, W.; Fang, R. H.; Zhang, L., Biomimetic Nanoemulsions for Oxygen Delivery In Vivo. *Adv. Mater.* **2018**, *30*, 1804693.

(31) Biffinger, J. C.; Kim, H. W.; DiMagno, S. G., The polar hydrophobicity of fluorinated compounds. *Chembiochem* **2004**, *5*, 622-627.

(32) Cheng, Y.; Cheng, H.; Jiang, C.; Qiu, X.; Wang, K.; Huan, W.; Yuan, A.; Wu, J.; Hu, Y., Perfluorocarbon nanoparticles enhance reactive oxygen levels and tumour growth inhibition in photodynamic therapy. *Nat. Commun.* **2015**, *6*, 8785.

(33) Yang, G.; Tian, J.; Chen, C.; Jiang, D.; Xue, Y.; Wang, C.; Gao, Y.; Zhang, W., An oxygen self-sufficient NIR-responsive nanosystem for enhanced PDT and chemotherapy against hypoxic tumors. *Chem. Sci.* **2019**, *10*, 5766-5772.

(34) Li, X.; Lee, S.; Yoon, J., Supramolecular photosensitizers rejuvenate photodynamic therapy. *Chem. Soc. Rev.* **2018**, *47*, 1174-1188.

(35) Li, S. Y.; Cheng, H.; Xie, B. R.; Qiu, W. X.; Zeng, J. Y.; Li, C. X.; Wan, S. S.; Zhang, L.; Liu, W. L.; Zhang, X. Z., Cancer Cell Membrane Camouflaged Cascade Bioreactor for Cancer Targeted Starvation and Photodynamic Therapy. *ACS Nano* **2017**, *11*, 7006-7018.

(36) Mao, D.; Hu, F.; Kenry; Ji, S.; Wu, W.; Ding, D.; Kong, D.; Liu, B., Metal-Organic-Framework-Assisted In Vivo Bacterial Metabolic Labeling and Precise Antibacterial Therapy. *Adv. Mater.* **2018**, *30*, 1706831.

(37) Wang, H.; Zhu, W.; Liu, J.; Dong, Z.; Liu, Z., pH-Responsive Nanoscale Covalent Organic Polymers as a Biodegradable Drug Carrier for Combined Photodynamic Chemotherapy of Cancer. *ACS Appl. Mater. Interfaces* **2018**, *10*, 14475-14482.

(38) Liu, S.; Liu, Y.; Hu, C.; Zhao, X.; Ma, P.; Pang, M., Boosting the antitumor efficacy over a nanoscale porphyrin-based covalent organic polymer via synergistic photodynamic and photothermal therapy. *Chem. Commun.* **2019**, *55*, 6269-6272.

(39) Wang, T.; Wang, D.; Yu, H.; Wang, M.; Liu, J.; Feng, B.; Zhou, F.; Yin, Q.; Zhang, Z.; Huang, Y.; Li, Y., Intracellularly Acid-Switchable Multifunctional Micelles for Combinational Photo/Chemotherapy of the Drug-Resistant Tumor. *ACS Nano* **2016**, *10*, 3496-3508.

(40) Dai, L. L.; Li, K.; Li, M. H.; Zhao, X. J.; Luo, Z.; Lu, L.; Luo, Y. F.; Cai, K. Y., Size/Charge Changeable Acidity-Responsive Micelleplex for Photodynamic-Improved PD-L1 Immunotherapy with Enhanced Tumor Penetration. *Adv. Funct. Mater.* **2018**, *28*, 1707249.

(41) Tang, Q. Y.; Xiao, W. Y.; Huang, C. H.; Si, W. L.; Shao, J. J.; Huang, W.; Chen, P.; Zhang, Q.; Dong, X. C., pH-Triggered and Enhanced Simultaneous Photodynamic and Photothermal Therapy Guided by Photoacoustic and Photothermal Imaging. *Chem. Mater.* **2017**, *29*, 5216-5224.

(42) Xu, Y.; Chen, J.; Tong, L.; Su, P.; Liu, Y.; Gu, B.; Bao, B.; Wang, L., pH/NIR-responsive semiconducting polymer nanoparticles for highly effective photoacoustic image guided chemo-photothermal synergistic therapy. *J. Controlled Release* **2019**, *293*, 94-103.

(43) Yang, Z.; Dai, Y.; Shan, L.; Shen, Z.; Wang, Z.; Yung, B. C.; Jacobson, O.; Liu, Y.; Tang, W.; Wang, S.; Lin, L.; Niu, G.; Huang, P.; Chen, X., Tumour microenvironment-responsive semiconducting polymer-based self-assembly nanotheranostics. *Nanoscale Horiz.* **2019**, *4*, 426-433.

(44) Fan, F.; Yu, Y.; Zhong, F.; Gao, M.; Sun, T.; Liu, J.; Zhang, H.; Qian, H.; Tao, W.; Yang, X., Design of Tumor Acidity-Responsive Sheddable Nanoparticles for Fluorescence/Magnetic Resonance Imaging-Guided Photodynamic Therapy. *Theranostics* **2017**, *7*, 1290-1302.

(45) Hu, X.; Zhang, Y.; Xie, Z.; Jing, X.; Bellotti, A.; Gu, Z., Stimuli-Responsive Polymersomes for Biomedical Applications. *Biomacromolecules* **2017**, *18*, 649-673.

(46) He, H.; Chen, Y.; Li, Y.; Song, Z.; Zhong, Y.; Zhu, R.; Cheng, J.; Yin, L., Effective and Selective Anti-Cancer Protein Delivery via All-Functions-in-One Nanocarriers Coupled with Visible Light-Responsive, Reversible Protein Engineering. *Adv. Funct. Mater.* **2018**, *28*, 1706710.

(47) Wang, J.; He, H.; Xu, X.; Wang, X.; Chen, Y.; Yin, L., Far-red light-mediated programmable anti-cancer gene delivery in cooperation with photodynamic therapy. *Biomaterials* **2018**, *171*, 72-82.

(48) Li, F.; Du, Y.; Liu, J.; Sun, H.; Wang, J.; Li, R.; Kim, D.; Hyeon, T.; Ling, D., Responsive Assembly of Upconversion Nanoparticles for pH-Activated and Near-Infrared-Triggered Photodynamic Therapy of Deep Tumors. *Adv. Mater.* **2018**, *30*, 1802808.

(49) Yu, Z.; Ge, Y.; Sun, Q.; Pan, W.; Wan, X.; Li, N.; Tang, B., A pre-protective strategy for precise tumor targeting and efficient photodynamic therapy with a switchable DNA/upconversion nanocomposite. *Chem. Sci.* **2018**, *9*, 3563-3569.

(50) Yang, G.; Xu, L.; Xu, J.; Zhang, R.; Song, G.; Chao, Y.; Feng, L.; Han, F.; Dong, Z.; Li, B.; Liu, Z., Smart Nanoreactors for pH-Responsive Tumor Homing, Mitochondria-Targeting, and Enhanced Photodynamic-Immunotherapy of Cancer. *Nano Lett.* **2018**, *18*, 2475-2484.

(51) Zhou, F.; Feng, B.; Yu, H.; Wang, D.; Wang, T.; Ma, Y.; Wang, S.; Li, Y., Tumor Microenvironment-Activatable Prodrug Vesicles for Nanoenabled Cancer Chemoimmunotherapy Combining Immunogenic Cell Death Induction and CD47 Blockade. *Adv. Mater.* **2019**, *31*, 1805888.

(52) Zhang, Y.; Dang, M.; Tian, Y.; Zhu, Y.; Liu, W.; Tian, W.; Su, Y.; Ni, Q.; Xu, C.; Lu, N.; Tao, J.; Li, Y.; Zhao, S.; Zhao, Y.; Yang, Z.; Sun, L.; Teng, Z.; Lu, G., Tumor Acidic Microenvironment Targeted Drug Delivery Based on pHLIP-Modified Mesoporous Organosilica Nanoparticles. *ACS Appl. Mater. Interfaces* **2017**, *9*, 30543-30552.

(53) Feng, B.; Zhou, F. Y.; Xu, Z. A.; Wang, T. T.; Wang, D. G.; Liu, J. P.; Fu, Y. L.; Yin, Q.; Zhang, Z. W.; Yu, H. J.; Li, Y. P., Versatile Prodrug Nanoparticles for Acid-Triggered Precise Imaging and Organelle-Specific Combination Cancer Therapy. *Adv. Funct. Mater.* **2016**, *26*, 7431-7442.

(54) Li, H.; Chen, Y.; Li, Z.; Li, X.; Jin, Q.; Ji, J., Hemoglobin as a Smart pH-Sensitive Nanocarrier To Achieve Aggregation Enhanced Tumor Retention. *Biomacromolecules* **2018**, *19*, 2007-2013.

(55) Xu, J. T.; Han, W.; Yang, P. P.; Jia, T.; Dong, S. M.; Bi, H. T.; Gulzar, A.; Yang, D.; Gai, S. L.; He, F.; Lin, J.; Li, C. X., Tumor Microenvironment-Responsive Mesoporous MnO2-Coated Upconversion Nanoplatform for Self-Enhanced Tumor Theranostics. *Adv. Funct. Mater*. **2018**, *28*, 1803804.

(56) Kim, W. L.; Cho, H.; Li, L.; Kang, H. C.; Huh, K. M., Biarmed poly(ethylene glycol)-(pheophorbide a)2 conjugate as a bioactivatable delivery carrier for photodynamic therapy. *Biomacromolecules* **2014**, *15*, 2224-2234.

(57) Staegemann, M. H.; Grafe, S.; Gitter, B.; Achazi, K.; Quaas, E.; Haag, R.; Wiehe, A., Hyperbranched Polyglycerol Loaded with (Zinc-)Porphyrins: Photosensitizer Release Under Reductive and Acidic Conditions for Improved Photodynamic Therapy. *Biomacromolecules* **2018**, *19*, 222-238.

(58) Zhu, K.; Liu, G.; Hu, J.; Liu, S., Near-Infrared Light-Activated Photochemical Internalization of Reduction-Responsive Polyprodrug Vesicles for Synergistic Photodynamic Therapy and Chemotherapy. *Biomacromolecules* **2017**, *18*, 2571-2582.

(59) Yan, L.; Miller, J.; Yuan, M.; Liu, J. F.; Busch, T. M.; Tsourkas, A.; Cheng, Z., Improved Photodynamic Therapy Efficacy of Protoporphyrin IX-Loaded Polymeric Micelles Using Erlotinib Pretreatment. *Biomacromolecules* **2017**, *18*, 1836-1844.

(60) Yang, Y.; Hou, W.; Liu, S.; Sun, K.; Li, M.; Wu, C., Biodegradable Polymer Nanoparticles for Photodynamic Therapy by Bioluminescence Resonance Energy Transfer. *Biomacromolecules* **2018**, *19*, 201-208.

(61) Yao, M.; Ma, Y.; Liu, H.; Khan, M. I.; Shen, S.; Li, S.; Zhao, Y.; Liu, Y.; Zhang, G.; Li, X.; Zhong, F.; Jiang, W.; Wang, Y., Enzyme Degradable Hyperbranched Polyphosphoester Micellar Nanomedicines for NIR Imaging-Guided Chemo-Photothermal Therapy of Drug-Resistant Cancers. *Biomacromolecules* **2018**, *19*, 1130-1141.

(62) Chen, H.; Tian, J.; He, W.; Guo, Z., H2O2-activatable and O2-evolving nanoparticles for highly efficient and selective photodynamic therapy against hypoxic tumor cells. *J. Am. Chem. Soc.* **2015**, *137*, 1539-1547.

(63) Zhu, H.; Li, J.; Qi, X.; Chen, P.; Pu, K., Oxygenic Hybrid Semiconducting Nanoparticles for Enhanced Photodynamic Therapy. *Nano Lett.* **2018**, *18*, 586-594.

(64) Ye, H.; Zhou, Y.; Liu, X.; Chen, Y.; Duan, S.; Zhu, R.; Liu, Y.; Yin, L., Recent Advances on Reactive Oxygen Species-Responsive Delivery and Diagnosis System. *Biomacromolecules* **2019**, *20*, 2441-2463.

(65) Yu, L.; Yang, Y.; Du, F. S.; Li, Z. C., ROS-Responsive Chalcogen-Containing Polycarbonates for Photodynamic Therapy. *Biomacromolecules* **2018**, *19*, 2182-2193.

(66) He, X.; Li, J.; An, S.; Jiang, C., pH-sensitive drug-delivery systems for tumor targeting. *Ther. Deliv.* **2013**, *4*, 1499-1510.

(67) Yang, Z.; Chen, Q.; Chen, J.; Dong, Z.; Zhang, R.; Liu, J.; Liu, Z., Tumor-pH-Responsive Dissociable Albumin-Tamoxifen Nanocomplexes Enabling Efficient Tumor Penetration and Hypoxia Relief for Enhanced Cancer Photodynamic Therapy. *Small* **2018**, *14*, 1803262.

(68) Feng, L. Z.; Dong, Z. L.; Tao, D. L.; Zhang, Y. C.; Liu, Z., The acidic tumor microenvironment: a target for smart cancer nano-theranostics. *Natl. Sci. Rev.* **2018**, *5*, 269-286.

(69) Li, H. J.; Du, J. Z.; Liu, J.; Du, X. J.; Shen, S.; Zhu, Y. H.; Wang, X.; Ye, X.; Nie, S.; Wang, J., Smart Superstructures with Ultrahigh pH-Sensitivity for Targeting Acidic Tumor Microenvironment: Instantaneous Size Switching and Improved Tumor Penetration. *ACS Nano* **2016**, *10*, 6753-6761.

(70) Xue, X.; Huang, Y.; Bo, R.; Jia, B.; Wu, H.; Yuan, Y.; Wang, Z.; Ma, Z.; Jing, D.; Xu, X.; Yu, W.; Lin, T. Y.; Li, Y., Trojan Horse nanotheranostics with dual transformability and multifunctionality for highly effective cancer treatment. *Nat. Commun.* **2018**, *9*, 3653.

(71) Ai, F.; Wang, N.; Zhang, X.; Sun, T.; Zhu, Q.; Kong, W.; Wang, F.; Zhu, G., An upconversion nanoplatform with extracellular pH-driven tumor-targeting ability for improved photodynamic therapy. *Nanoscale* **2018**, *10*, 4432-4441.

(72) Mo, R.; Sun, Q.; Xue, J.; Li, N.; Li, W.; Zhang, C.; Ping, Q., Multistage pH-responsive liposomes for mitochondrial-targeted anticancer drug delivery. *Adv. Mater.* **2012**, *24*, 3659-3665.

(73) Mi, P.; Kokuryo, D.; Cabral, H.; Wu, H.; Terada, Y.; Saga, T.; Aoki, I.; Nishiyama, N.; Kataoka, K., A pH-activatable nanoparticle with signal-amplification capabilities for non-invasive imaging of tumour malignancy. *Nat. Nanotechnol.* **2016**, *11*, 724-730.

(74) Wang, Y.; Zhou, K.; Huang, G.; Hensley, C.; Huang, X.; Ma, X.; Zhao, T.; Sumer, B. D.; DeBerardinis, R. J.; Gao, J., A nanoparticle-based strategy for the imaging of a broad range of tumours by nonlinear amplification of microenvironment signals. *Nat. Mater.* **2014**, *13*, 204-212.

(75) Xiong, H.; Zhou, K.; Yan, Y.; Miller, J. B.; Siegwart, D. J., Tumor-Activated Water-Soluble Photosensitizers for Near-Infrared Photodynamic Cancer Therapy. *ACS Appl. Mater. Interfaces* **2018**, *10*, 16335-16343.

(76) Zheng, X. H.; Wang, L.; Liu, S.; Zhang, W.; Liu, F. G.; Xie, Z. G., Nanoparticles of Chlorin Dimer with Enhanced Absorbance for Photoacoustic Imaging and Phototherapy. *Adv. Funct. Mater.* **2018**, *28*, 1706507.

(77) Li, B.; Lin, L.; Lin, H.; Wilson, B. C., Photosensitized singlet oxygen generation and detection: Recent advances and future perspectives in cancer photodynamic therapy. *J Biophotonics.* **2016**, *9*, 1314-1325.

Table of Content